

Theoretical study on the mechanism for the excited-state double proton transfer process of an asymmetric Schiff base ligand

Zhengran Wang(王正然), Qiao Zhou(周悄), Bifa Cao(曹必发), Bo Li(栗博), Lixia Zhu(朱丽霞),Xinglei Zhang(张星蕾), Hang Yin(尹航), and Ying Shi(石英)

Citation: Chin. Phys. B, 2022, 31 (**4**): 048202. DOI: 10.1088/1674-1056/ac21c2
Journal homepage: http://cpb.iphy.ac.cn; http://iopscience.iop.org/cpb

What follows is a list of articles you may be interested in

A DFT/TD-DFT study of effect of different substituent on ESIPT fluorescence features of 2-(2'-hydroxyphenyl)-4-chloro- methylthiazole derivatives

Shen-Yang Su(苏申阳), Xiu-Ning Liang(梁秀宁), and Hua Fang(方华)
Chin. Phys. B, 2022, 31 (**3**): 038202. DOI: 10.1088/1674-1056/ac21c6

Influence of intramolecular hydrogen bond formation sites on fluorescence mechanism

Hong-Bin Zhan(战鸿彬), Heng-Wei Zhang(张恒炜), Jun-Jie Jiang(江俊杰), Yi Wang(王一), Xu Fei(费旭), and Jing Tian(田晶)
Chin. Phys. B, 2022, 31 (**3**): 038201. DOI: 10.1088/1674-1056/ac29ad

Theoretical investigation of fluorescence changes caused bymethanol bridge based on ESIPT reaction

Xinglei Zhang(张星蕾), Lixia Zhu(朱丽霞), Zhengran Wang(王正然), Bifa Cao(曹必发), Qiao Zhou(周悄), You Li(李尤), Bo Li(栗博), Hang Yin(尹航), and Ying Shi(石英)
Chin. Phys. B, 2021, 30 (**11**): 118202. DOI: 10.1088/1674-1056/abf131

Relationship between ESIPT properties and antioxidant activities of 5-hydroxyflavone derivates

Chaofan Sun(孙朝范), Bifa Cao(曹必发), Hang Yin(尹航), Ying Shi(石英)
Chin. Phys. B, 2020, 29 (**5**): 058202. DOI: 10.1088/1674-1056/ab7ea1

Theoretical study on the relationship between the position of the substituent and the ESIPT fluorescence characteristic of HPIP

Xin Zhang(张馨), Jian-Hui Han(韩建慧), You Li(李尤), Chao-Fan Sun(孙朝范), Xing Su(苏醒), Ying Shi(石英), Hang Yin(尹航)
Chin. Phys. B, 2020, 29 (**3**): 038201. DOI: 10.1088/1674-1056/ab6d50

Theoretical study on the mechanism for the excited-state double proton transfer process of an asymmetric Schiff base ligand

Zhengran Wang(王正然), Qiao Zhou(周悄), Bifa Cao(曹必发), Bo Li(栗博), Lixia Zhu(朱丽霞), Xinglei Zhang(张星蕾), Hang Yin(尹航), and Ying Shi(石英)†

Institute of Atomic and Molecular Physics, Jilin University, Changchun 130012, *China*

(Received 16 July 2021; revised manuscript received 15 August 2021; accepted manuscript online 27 August 2021)

Excited-state double proton transfer (ESDPT) in the 1-[(2-hydroxy-3-methoxy-benzylidene)-hydrazonomethyl]-naphthalen-2-ol ($HYDRAVH_2$) ligand was studied by the density functional theory and time-dependent density functional theory method. The analysis of frontier molecular orbitals, infrared spectra, and non-covalent interactions have cross-validated that the asymmetric structure has an influence on the proton transfer, which makes the proton transfer ability of the two hydrogen protons different. The potential energy surfaces in both S_0 and S_1 states were scanned with varying O–H bond lengths. The results of potential energy surface analysis adequately proved that the $HYDRAVH_2$ can undergo the ESDPT process in the S_1 state and the double proton transfer process is a stepwise proton transfer mechanism. Our work can pave the way towards the design and synthesis of new molecules.

Keywords: DFT/TDDFT, schiff base ligand, excited state intramolecular double proton transfer

PACS: 82.39.Jn, 31.15.ee, 87.15.ht **DOI:** 10.1088/1674-1056/ac21c2

1. Introduction

Photoexcited proton transfer has been investigated intensively both experimentally and theoretically, because of its important role in physical and biological systems.[1–3] The first discovered excited state proton transfer phenomenon was discovered by Weller and co-workers in the characteristic experiment of methyl salicylate.[4] Molecules with excited state intramolecular proton transfer (ESIPT) properties could exhibit dual fluorescence peaks under specific photo-excitation.[5,6] One of the fluorescence peaks could derive from the initial molecular structure before ESIPT behavior (enol configuration), and the other one results from the form after ESIPT reaction (keto structure).[7] In general, most ESIPT reactions are involved with single proton transfer. However, such a single proton transfer could not be sufficient to simulate the proton transfer process thoroughly in the biological field, because the most photoinduced mutation of DNA or RNA refers to double or multiple protons participating.[8–12] Taylor *et al.* found that the 7-azaindole dimer has a different tautomer in the ground and first excited states, which is the first recorded example of concerted double proton transfer.[13] Since then, the excited state double proton transfer (ESDPT) process has been extensively investigated due to its potential applications in chemical reactions and alkaloid base pair variation.[14–17]

Schiff base ligands with proton transfer properties have been studied extensively due to their thermal, photochromatic, complex properties and tautomeric equilibrium.[18–22] They are classified as symmetric and asymmetric ligand based on contracture. Asymmetric Schiff base ligands can provide appropriate donor sets capable of holding three metal ions in a linear complex. Recently, asymmetric Schiff base ligands have been attracting considerable attraction, which are very useful ligands in the synthesis of transition metal complexes.[23–28] Samira *et al.* synthesized 1-[(2-hydroxy-3-methoxy-benzylidene)-hydrazonomethyl]-naphthalen-2-ol($HYDRAVH_2$) ligand.[29] $THYDRAVH_2$ is an asymmetric fluorescence Schiff base ligand with the properties of ESDPT and remarkable optical properties. In Samira *et al.*'s study, the structure of the $HYDRAVH_2$ was characterized. And the experimental results indicate that the $HYDRAVH_2$ ligand displays particularly enhanced emission properties in near-infrared, and has great application value in optoelectronic devices. It can be used to synthesize a series of new fluorescent lanthanide (III) complexes which caused an increase in fluorescence.[30] Due to the asymmetry of its structure, it has a certain impact on the double proton transfer. However, the mechanism of the ESDPT process in the $HYDRAVH_2$ system is still unclear.

In the present work, we optimized the structures of the HYDRAVH2 in S_0 state and S_1 state by the density functional theory (DFT) method and the time-dependent DFT (TDDFT) method, respectively. Moreover, the non-covalent interactions, frontier molecular orbitals and potential energy surfaces were presented to explore the double proton transfer mechanism.

2. Theoretical calculation methods

In this work, the related calculations were completed on the Gaussian 09 program suit.[31] The ground- and excited-state geometric configurations of the $HYDRAVH_2$ monomer

†Corresponding author. E-mail: shi_ying@jlu.edu.cn

© 2022 Chinese Physical Society and IOP Publishing Ltd

in enol and keto forms were optimized in the framework of DFT and TD-DFT methods, respectively, with the B3LYP functional and 6-311 + G(d) basis set.[32,33] The 1H NMR spectra of structure was done on the optimized geometries at the same computational level. The 1H NMR chemical shifts of the $HYDRAVH_2$ were predicted with respect to the tetramethyl silane (TMS) by employing the gauge-independent atomic orbital method.[34–36] In view of the acetonitrile (ACN) solvent adopted in previous experiment, the ACN solvent with integral equation formalism variant of the polarizable continuum model (IEFPCM) was used in theoretical arithmetic.[37,38] Based on the optimized configurations, the pivotal bond lengths, bond angles, frontier molecular orbitals, absorption and emission properties, and infrared (IR) vibration spectra were calculated.[39] The reduced density gradient (RDG) images were drawn by Multiwfn software.[40–42] In view of adopting potential energy curves to illustrate the ESDPT mechanisms, the S_0 and S_1 potential energy curves have been scanned by increasing the bond length of O_{22}–H_{34} and O_{11}–H_{39} in steps of 0.1 Å.

3. Results and discussion

3.1. Optimized geometric structures

The ground- and excited-state geometric configurations of the $HYDRAVH_2$ monomer in enol forms are optimized as shown in Fig. 1. The bond lengths (O–H and H–N) and bond angles δ(O–H···N) related to the hydrogen bond are summarized in Table 1. In the S_0 state, the bond lengths of O_{22}–H_{34}, $N_{14}\cdots H_{34}$, O_{11}–H_{39}, and $N_{13}\cdots H_{39}$ are 0.98 Å, 1.78 Å, 0.99 Å, and 1.72 Å, respectively. When the $HYDRAVH_2$ is photoexcited to S_1 state, these bond lengths change to 0.99 Å, 1.73 Å, 1.00 Å, and 1.69 Å, respectively. It is found that compared with S_0 state, the bond lengths of O_{22}–H_{34} and O_{11}–H_{39} increased in S_1 state, while the bond lengths of $N_{14}\cdots H_{34}$ and $N_{13}\cdots H_{39}$ shortened in S_1 state. Due to the asymmetry of the $HYDRAVH_2$ structure, the change value of the bond length of the two hydrogen bonds that can promote proton transfer is different. That is to say, the proton transfer abilities of H_{34} and H_{39} are contrasting.

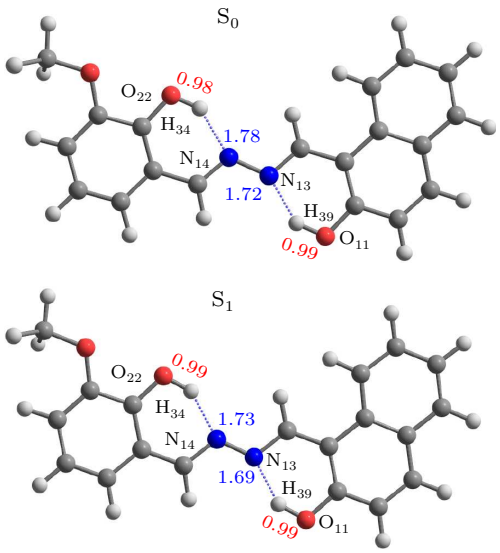


Fig. 1. The optimized ground and excited states structures of $HYDRAVH_2$.

Table 1. Obtained bond lengths (Å) and bond angles (°) of the $HYDRAVH_2$ in the S_0 and S_1 states, respectively.

Atoms	O_{22}–H_{34}	N_{14}–H_{34}	$\delta(O_{22}$–$H_{34}\cdots N_{14})$	O_{11}–H_{39}	N_{13}–H_{39}	$\delta(O_{11}$–$H_{39}\cdots N_{13})$
S_0	0.98	1.78	144.97	0.99	1.72	144.71
S_1	0.99	1.73	146.90	1.00	1.69	146.75

Table 2. Chemical shift values (ppm) in 1H NMR spectra of $HYDRAVH_2$ determined experimentally and theoretically by the B3LYP/6-311 + G(d) level and IEFPCM model. The calculated chemical shift data for $HYDRAVH_2$.

Atoms	Experimental chemical shift (ppm)[29]	B3LYP/6-311 +G(d) GIAO	Atoms	Experimental chemical shift (ppm)[29]	B3LYP/6-311 +G(d) GIAO
H24	9.08	8.895	H29	7.33	7.450
H25	8.64	8.446	H30	8.04	8.211
H26	7.63	7.923	H31	9.88	9.830
H27	7.45	7.681	H32	7.27	7.114
H28	7.92	8.087	H33	7.16	7.114
H34	–	10.478	H39	–	11.459
H36, H37, H38	3.86	3.993	H40	6.69	7.038

3.2. The 1H NMR spectra

The NMR spectroscopy is a powerful tool for the direct detection of chemical species and forms of molecular interactions in complex materials.[43] The 1H NMR spectra calculation of $HYDRAVH_2$ is shown in Table 2, which quite agreed with experimental NMR spectra.[29] The calculated isotropic shielding tensor for TMS is equal to 31.94 ppm for the 1H nuclei.[44] The chemical shifts of all involved protons are listed in Table 2. Similarly, the calculated proton chemical shifts of H39 and H34 are arrived at 11.459 ppm and 10.478 ppm, respectively. The calculated NMR chemical shift values are in good agreement with the experimental values. The results

confirm the reliability of the calculated method we have chosen. In addition, it is worth noting that for all protons of $HYDRAVH_2$, H34 and H39 shift the most considerably, suggesting there are two strong hydrogen bond interactions in O–H···N. And the strength of the two hydrogen bonds is distinct.

3.3. Non-covalent interaction analysis

Yang *et al.* introduced a method for imagining non-covalent interactions in real space,[45] which could explore intramolecular interactions. The different types of interaction and the homologous intensities can be definitely shown by analyzing the electron densities ($\rho(r)$) and their RDG isosurfaces. Specifically, the expression is

$$\mathrm{RDG}(r) = \frac{1}{2(3\pi^2)^{4/3}} \frac{|\nabla\rho(r)|}{\rho(r)^{4/3}}. \tag{1}$$

According to Bader's Atoms in molecules theory,[46] the relative to the second largest eigenvalue λ_2 of Hessian matrix of electron density and the total electron density may be written in

$$\Omega(r) = \mathrm{sign}(\lambda_2(r))\,\rho(r). \tag{2}$$

The eigenvalue $\lambda_2 > 0$ acts for bonding interactions and the $\lambda_2 < 0$ represents anti-bonding interactions. The $\Omega(r)$ negative value stands for hydrogen bond interaction. In contrast, the positive value of $\Omega(r)$ means the presence of the steric hindrance. A nearly zero value of sign $\Omega(r)$ indicates weak interactions. The scatter plots for the RDG value versus the $\Omega(r)$ value of $HYDRAVH_2$ in the ground-state and excited-state are shown in Fig. 2. The colors from blue to red indicate the $\Omega(r)$ value from negative to positive. As shown in Fig. 2, the two spike peaks of the $HYDRAVH_2$ are observed and located at -0.045 and -0.051, respectively, in the S_0 state. The two spike peaks are assigned to O_{11}–$H_{39}\cdots N_{13}$ (-0.045) and O_{22}–$H_{34}\cdots N_{14}$ (-0.051), respectively. Upon photoexcitation to the S_1 state, O_{11}–$H_{39}\cdots N_{13}$ and O_{22}–$H_{34}\cdots N_{14}$ both shift from -0.045 to -0.050 and from -0.051 to -0.056. The left shift proves that the strength of two hydrogen bonds interaction in the $HYDRAVH_2$ increases in S_1 state. It is obvious that the intensity of interactions O_{22}–$H_{34}\cdots N_{14}$ is stronger than O_{11}–$H_{39}\cdots N_{13}$. It can be concluded that the double transfer may not be synchronous in the excited state.

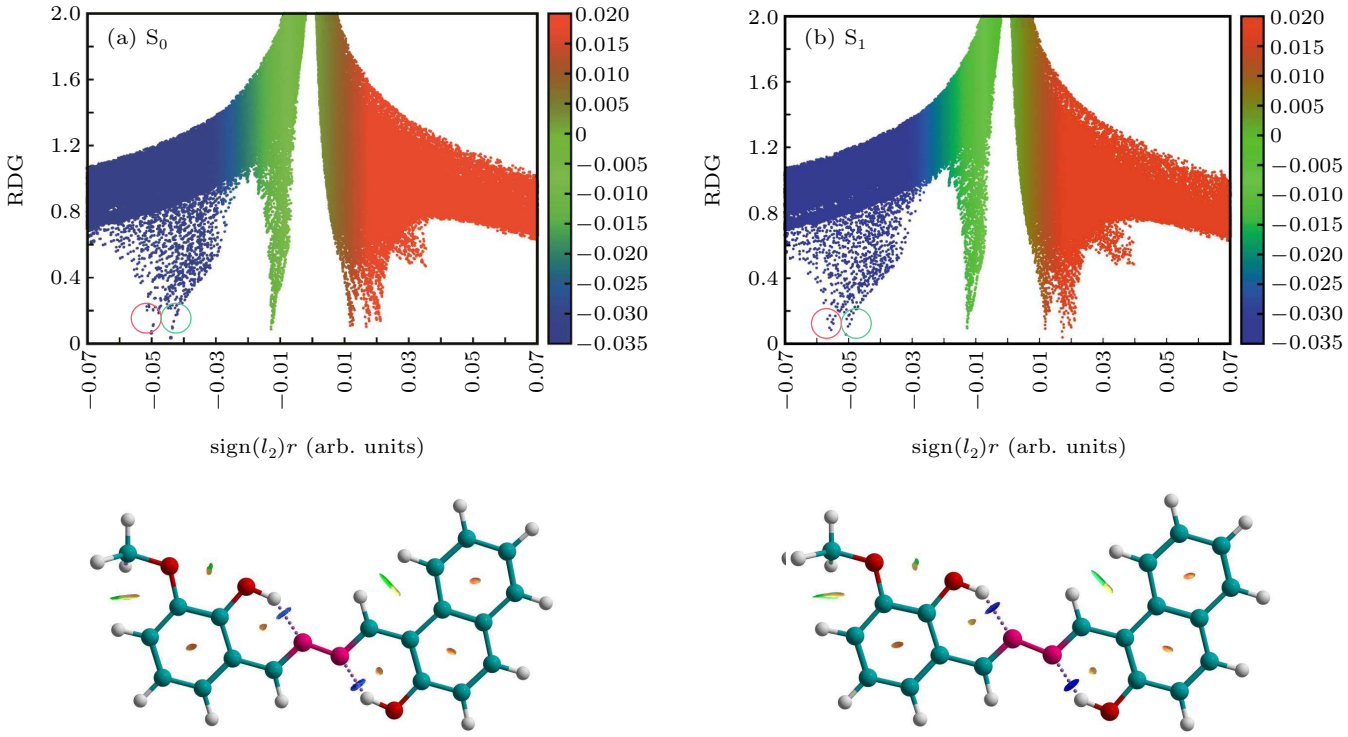


Fig. 2. Plots of function value 1 versus function value 2 for $HYDRAVH_2$ in (a) S_0 and (b) S_1 states, as well as the assignments of each spike by gradient isosurfaces.

3.4. Frontier molecular orbitals

The frontier molecular orbital can reflect the distribution of electron density before and after molecular excitation clearly.[47] Figure 3 shows the electron density distribution of the highest occupied molecular orbital (HOMO) and the lowest unoccupied molecular orbital (LUMO) for the $HYDRAVH_2$ in the enol and keto states. It can be found from Fig. 3 that the HOMO and the LUMO are characterized by the π and π^* features, respectively. Herein, we just concentrate on the charge redistribution around hydrogen bonding moieties, which can affect excited state hydrogen bonding dynamics seriously. The electronic densities around O_{22} and O_{11} on HOMO orbital decrease compared with those on LUMO orbital, while the electronic densities around N atoms

increase instead. This has significant facilitate effects on moving the hydrogen protons to the proton acceptors. Therefore, hydrogen bonds are strengthened in the photoexcitation process. Crucially, we can see that the change in electron density around O_{22} is more pronounced than around O_{11}, indicating that more electrons are transferred. Due to the difference in charge distribution around the donor O_{22} and O_{11}, the two oxygen donors have different driving forces for proton transfer, which directly leads to the fact that H_{34} and H_{39} cannot be transferred simultaneously.

Furthermore, by comparing the frontier molecular orbitals of the three keto states, we find that the strong coupling effect between the HOMO and LUMO happens in the keto1 form. However, when the $HYDRAVH_2$ is in the keto2 or keto3 state, the coupling degree of charge between HOMO and LUMO orbitals is lower than that of keto1 obviously.

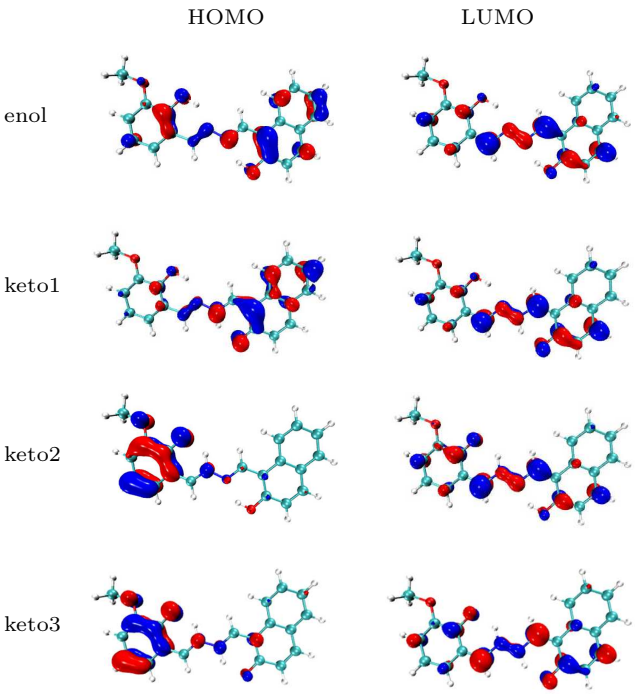


Fig. 3. The frontier molecular orbitals (HOMO and LUMO) of the $HYDRAVH_2$ in the enol state and keto state.

3.5. Absorption and emission spectra

The theoretical absorption peak and emission spectra of $HYDRAVH_2$ in ACN solvent are calculated as shown in Fig. 4. It can be seen from Fig. 4 that the absorption peaks of the $HYDRAVH_2$ are located at 338 nm and 397 nm, which stay closely aligned with the experimental results (332 nm and 387 nm).[30] We calculated two emission peaks and classified them as keto1 form and keto2 form, exhibiting the red shifts compared to the absorption peaks. The calculated emission peak of keto1 is 514 nm, which is in good agreement with the experimental values (495 nm).[30] In addition, we also calculated an emission peak of the keto2 form located at 664 nm. But in fact, only a single fluorescence emission was observed in the experiment. Combined with the frontier molecular orbital analysis above, the decouple effect between the electronic donor and the acceptor is a main factor for the nonfluorescent phenomenon.[48] Thus, we infer that the single fluorescence observed in the experiment should originate from the keto1 state, while the fluorescence cannot be emitted from the keto2 and keto3 states.

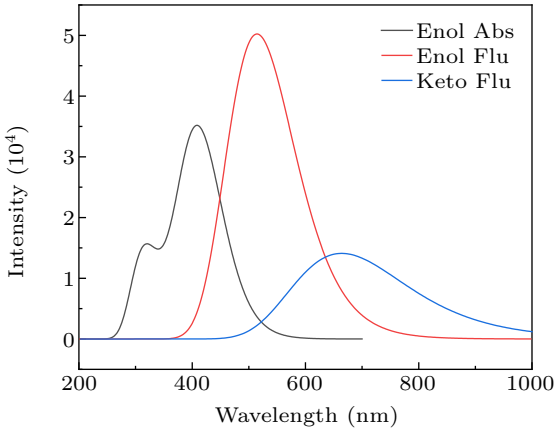


Fig. 4. The theoretical absorption peaks and calculated emission spectra of the $HYDRAVH_2$.

3.6. IR vibration spectra

The calculation results of the IR spectra of the $HYDRAVH_2$ in the S_0 state and the S_1 state are shown in Fig. 5. It can be seen that the O_{22}–H_{34} and O_{11}–H_{39} stretching peaks of $HYDRAVH_2$ in the S_0 state are located at 3276 cm^{-1} and 3165 cm^{-1}, exhibiting a red shift of 230 cm^{-1} and 195 cm^{-1} to 3046 cm^{-1} and 2970 cm^{-1} in the S_1 state, respectively. The red shift of the O–H stretching peaks for the $HYDRAVH_2$ suggests that the hydrogen bonds O–H$\cdots$N are all strengthened in the S_1 state, promoting the occurrence of ESDPT.[49] Furthermore, it shows that in this state, the vibration frequency between O_{22}–H_{34} is stronger than that between O_{11}–H_{39}, indicating that the hydrogen bond of the former is stronger.

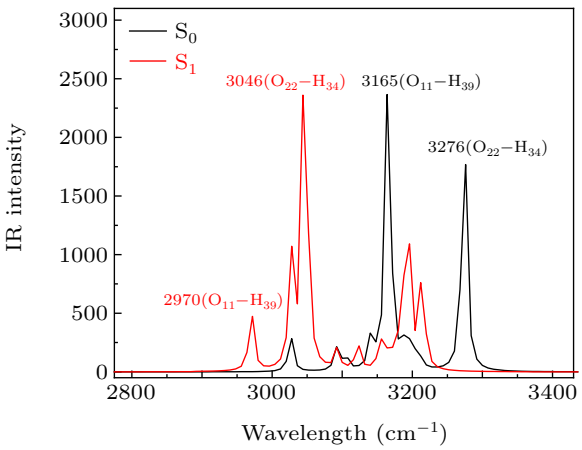


Fig. 5. The calculated IR spectra of $HYDRAVH_2$ in the S_0 and S_1.

3.7. Potential energy surfaces

In order to reveal the excited state intramolecular double proton transfer mechanism of the $HYDRAVH_2$ clearly, we constructed the potential energy surfaces of the $HYDRAVH_2$ in the S_0 state and the S_1 state.[50] The potential energy surfaces are scanned for molecule $HYDRAVH_2$ in S_0 and S_1 states with various bond lengths of O_{22}–H_{34} and O_{11}–H_{39} from 0.99 Å to 2.09 Å in steps of 0.1 Å and are shown in Fig. 6.

As shown in Fig. 6(a), in the ground state, the relationship of the four minima potential energy is $E_B = E_C > E_D > E_A$. Points *B*, *C* and *D* in the figure correspond to keto1, keto2 and keto3 of the optimized configuration, respectively. The potential energy barriers among these points are calculated and presented as follows: 7.67 kcal/mol is needed to cross point *A* to reach point *B* (or *C*), the proton transfer from the enol (point *A*) structure to the keto structure (point *D*) needs to cross an energy barrier of 11.32 kcal/mol. Due to the high energy barrier of proton transfer, it is difficult for $HYDRAVH_2$ to spontaneously carry out the intermolecular double proton transfer process in the S_0 state.[51]

Figure 6(b) shows the potential energy surface of the $HYDRAVH_2$ in the S_1 state. After excitation to the S_1 state, four structures denoted *A*, *B*, *C*, and *D* are observed. Among them, point *A* represents the enol structure of the $HYDRAVH_2$, point *B* and point *C* represent the single proton transfer structure of the $HYDRAVH_2$, point *D* represents the keto structure of the $HYDRAVH_2$ after double proton transfer. The obvious decrease of energy barrier after photoexcitation indicates that the strengthening of the intramolecular hydrogen bond can promote the proton transfer. As shown in Fig. 6(b), $HYDRAVH_2$ has the following three pathways to complete the excited state double proton transfer process, namely, $A \rightarrow B \rightarrow D$, $A \rightarrow C \rightarrow D$, and $A \rightarrow D$. Among them, the first two paths are the stepwise proton transfer mechanism, and the third is the cooperative proton transfer mechanism. Specifically, the potential energy barriers among these points are calculated and presented as follows: the $HYDRAVH_2$ needs to cross the energy barrier of 4.65 kcal/mol from point *A* to point *B* and 2.43 kcal/mol from point *A* to point *C*. Then a higher barrier (6.43 kcal/mol) is required to reach the *D* point from the *A* point. The two energy barriers are low enough for the proton transfer. However, it is difficult for the two protons to transfer simultaneously because of the higher barrier from point *A* to point *D*. It can be deduced that the double protons are transferred stepwise. Compared with $A \rightarrow B$ process, the energy barrier needs to be crossed in $A \rightarrow C$ process is lower, it shows that the $A \rightarrow C$ process is more prone to proton transfer. These results identify that the $HYDRAVH_2$ can undergo ESDPT process in the first excited state and the transfer mechanism is a stepwise transfer mechanism.

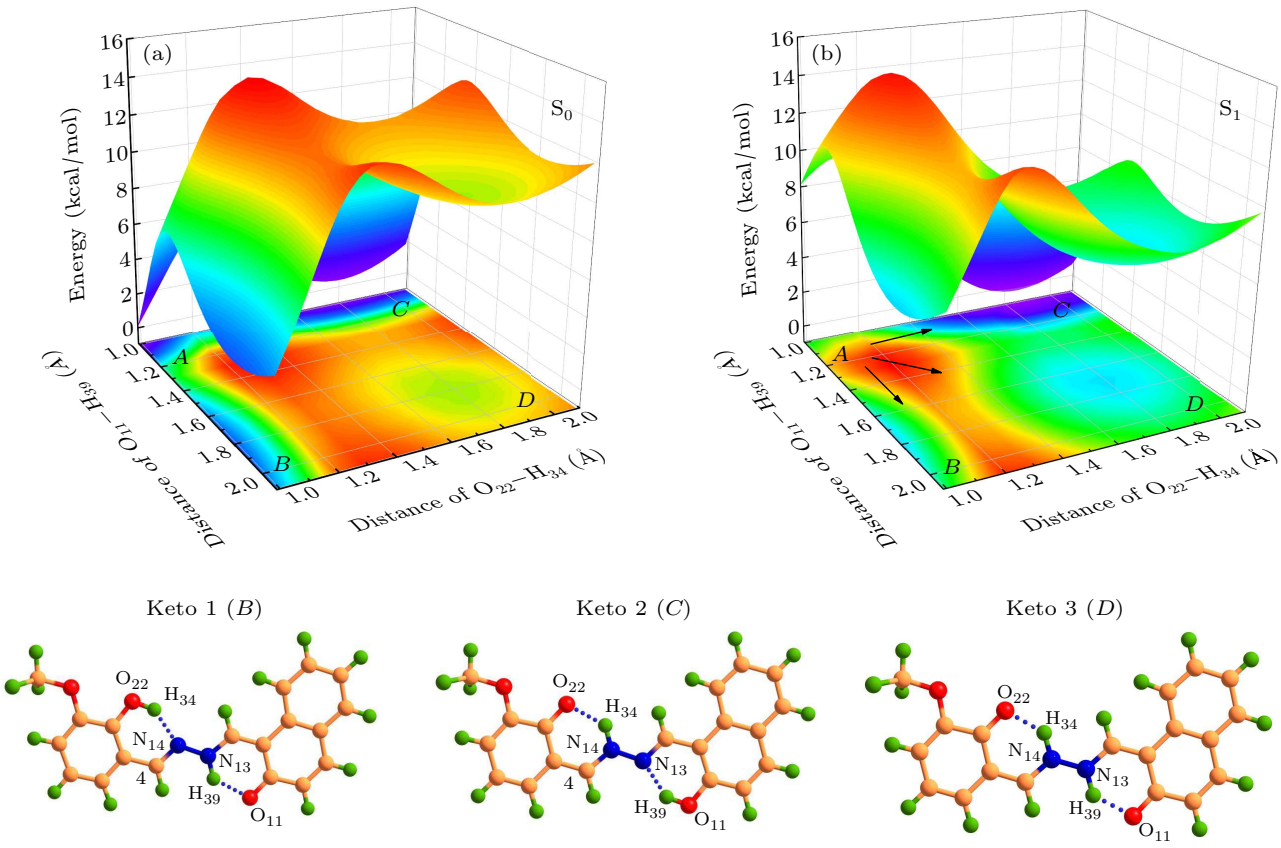


Fig. 6. Potential energy surfaces of the (a) ground and (b) first excited states for $HYDRAVH_2$ molecule along O_{22}–H_{34} and O_{11}–H_{39} bond lengths and the three possible configurations in the keto form.

4. Conclusion

Summing up, the excited state intramolecular double proton transfer of HYDRAVH$_2$ is theoretically investigated by DFT and TDDFT methods. The results of our investigation fully confirm that H_{34} and H_{39} have different proton transfer abilities by comparing the changes in the primary bond parameters. Frontier molecular orbital analysis shows that the increased charge densities on proton acceptor moiety could promote the ESDPT process. Furthermore, the IR vibration spectrum and the non-covalent interaction analysis further confirm the tendency of the ESDPT process. The results of potential energy surface analysis adequately prove the double proton transfer process is a stepwise proton transfer mechanism by comparing the heights of energy barriers. These distinctive characteristics provide valuable guidance for controlling the ESDPT process as well as the design and synthesis of new Schiff base ligands.

Acknowledgments

Project supported by the National Basic Research Program of China (Grant No. 2019YFA0307701), the National Natural Science Foundation of China (Grant No. 11874180), and the Young and Middle-aged Scientific and Technological Innovation leaders and Team Projects in Jilin Province, China (Grant No. 20200301020RQ).

References

[1] Karas L J, Wu C H, Ottosson H and Wu J I 2020 *Chem. Sci.* **11** 10071
[2] Sun C F, Li Y, Li B, Han J H, Zhou Q, Yin H and Shi Y 2020 *J. Mol. Liq.* **297** 111937
[3] Mu X J, Wang J G and Sun M T 2019 *J. Phys. Chem. C* **123** 14132
[4] Weller A 1956 *Z. Elektrochem.* **60** 1144
[5] Yang G, Chen K F, Wang G and Yang D P 2020 *Chin. Phys. B* **29** 103103
[6] Yang Y G, Liu Y, Liu Y F and Jiang K 2020 *J. Lumin.* **227** 117587
[7] Zhang X, Han J H, Li Y, Sun C F, Su X, Shi Y and Yin H 2020 *Chin. Phys. B* **29** 038201
[8] Wang J M, Liu Q and Yang D P 2020 *Sci. Rep.* **10** 5119
[9] Xie Z, Yang B, Li F, Cheng G, Liu L, Yang G, Xu H, Ye L, Hanif M, Liu S, Ma D and Ma Y 2005 *J. Am. Chem. Soc.* **127** 14152
[10] Xu L, Zhang T J, Zhang Q L and Yang D P 2020 *Chin. Phys. B* **29** 053102
[11] Zhou Q, Du C, Yang L, Zhao M, Dai Y and Song P 2017 *J. Phys. Chem. A* **121** 4645
[12] Yin H and Shi Y 2018 *Chin. Phys. B* **27** 058201
[13] Taylor C A, El-Bayoumi M A and Kasha M 1969 *Proc. Natl. Acad. Sci. USA* **63** 253
[14] Tanner C, Manca C and Leutwyler S 2003 *Science* **302** 1736
[15] Zhao J, Chen J, Cui Y, Wang J, Xia L, Dai Y, Song P and Ma F 2015 *Phys. Chem. Chem. Phys.* **17** 1142
[16] Chou P T, Wei C Y, Chang C P and Chiu C H 1995 *J. Am. Chem. Soc.* **117** 7259
[17] Ma C, Yang Y G, Li C Z and Liu Y F 2015 *J. Phys. Chem. A* **119** 12686
[18] Takeuchi S and Tahara T 2007 *Proc. Natl. Acad. Sci. USA* **104** 5285
[19] Jayachandrabal B and Thirugnanasambandam S 2020 *J. Microencapsul.* **37** 29
[20] Sahraei A, Kargar H, Hakimi M and Tahir M N 2017 *J. Mol. Struct.* **1149** 576
[21] Kenan B and Metin Ö 2020 *J. Mol. Struct.* **1202** 127266
[22] Petar T, Stela G, Petia P, Rusi R, Boris S and Anton G 2020 *New J. Chem.* **44** 15081
[23] Youka B, Yuta T, Masahiro K, Tatsuhiko Y and Shigeki M 2021 *ACS Catal.* **11** 2663
[24] Gao B J, Zhang D D and Don T T 2015 *J. Phys. Chem. C* **119** 16403
[25] Weng Q H, Yi J Q, Chen X P, Luo D W, Wang Y D, Sun W M, Kang J and Zhong Z 2020 *ACS Omega.* **5** 24864
[26] Mu X J and Sun M T 2020 *Appl. Phys. Lett.* **117** 091601
[27] Yang Y G, Liu Y, Zhai H S, Jia X L, He Y Y, Ma Q F, Zhang R G, Liu Y F and Jiang K 2020 *J. Lumin.* **223** 117224
[28] Zhu W T, Ma S H, Fang J P, Ma Z Y and Zhu H P 2014 *Chin. Phys. B* **23** 060505
[29] Samira G D, Hamid K and Carolina E S 2017 *Polyhedron* **133** 48
[30] Samira G D, Janet S and Carolina E S 2020 *J. Mol. Struct.* **1219** 129060
[31] Shang C J, Sun C F, Li Y Z 2021 *J. Mol. Struct.* **1236** 130370
[32] Shang X H, Han D M, Zhan Q, Zhang G, and Li D F 2014 *Organometallics* **33** 3300
[33] Ding J X, D H Shi, Sun J F and Liu Y F 2008 *J. Phys. Chem. A* **112** 6244
[34] Shang C J, Cao Y J, Sun C F, Li Y Z 2021 *J. Lumin.* **235** 118059
[35] Haroldo C D S and Wagner B D A 2020 *Chem. Phys.* **528** 110479
[36] Yang Y G, Zhai H S, Liu Y, Jia X L, He Y Y, Ma Q F, Zhang R G, Liu Y F and Jiang K 2019 *J. Lumin.* **216** 116736
[37] Mónica A G, Norma F H, Marco G, Erasmo O B and Daniel G M 2010 *J. Mol. Struct.* **945** 101
[38] Lyudmila O K, Svetlana V L and Victor V K 2021 *Optik-International Journal for Light and Electron Optics* **242** 167156
[39] Song P, Li Y Z, Ma F C, Pullerits T and Sun M T 2013 *J. Phys. Chem. C* **117** 15879
[40] Sidra K, Hasnain S, Khurshid A and Tariq M 2020 *J. Mol. Liq.* **316** 113860
[41] Li X, Guo Y Y and Yang D P 2020 *Theor. Chem. Acc.* **139** 181
[42] Feride A, Noureddine I and Aleksandr S K 2020 *J. Mol. Model.* **26** 161
[43] Jan V, Gabriel D and Radek M 2012 *Inorg. Chem.* **51** 1371
[44] Randi P A S, Moreira G M and Bettega M H F 2020 *Phys. Rev. A* **102** 022812
[45] Andrew J N, Margaret J H, Matthew S S and Dean T F 2017 *Nature* **543** 637
[46] Christian T 2018 *Theor. Chem. Acc.* **137** 93
[47] Mao Y Z, Martin H G and Shao Y H 2018 *Chem. Sci.* **9** 8598
[48] Li H, Han J H, Zhao H F, Liu X C, Luo Y, Shi Y, Liu C L, Jin M X and Ding D J 2019 *J. Phys. Chem. Lett.* **10** 748
[49] Yang Y G, Li D L, Li C Z, Liu Y F and Jiang K 2018 *J. Hazard. Mater.* **341** 93
[50] Lionel L, Norah M H and Neepa T M 2019 *Phys. Rev. Lett.* **123** 083201
[51] Zhang Y Y, Shi Y and Li Y Z 2016 *J Mater Sci: Mater Electron* **27** 7132